ORIGINAL PAPER

Electrochemical polymerization of polyaniline doped with Zn^{2+} as the electrode material for electrochemical supercapacitors

Hui Xu · Junlong Zhang · Yong Chen · Hailin Lu · Junxia Zhuang

Abstract Polyaniline doped with Zn^{2+} (PANI/Zn^{2+}) films was synthesized by cyclic voltammetric method on stainless steel mesh substrates in 0.2 mol L^{-1} aniline and 0.5 mol L^{-1} sulfuric acid electrolyte with various concentrations of zinc sulfate ($ZnSO_4·7H_2O$). The structure and morphology of PANI and PANI/Zn^{2+} films were characterized by Fourier transform infrared, X-ray diffraction, scanning electron microscopy, energy-dispersive X-ray spectroscopy, and X-ray photoelectron spectroscopy techniques, respectively. The electrochemical properties of PANI and PANI/Zn^{2+} films were investigated by cyclic voltammetry, galvanostatic charge–discharge test, and electrochemical impedance spectroscopy in 0.5 mol L^{-1} H_2SO_4 electrolyte in a three-electrode system. The results show that the surface morphology of PANI/Zn^{2+} is more rough than that of pure PANI. The specific capacitance of the PANI/Zn^{2+} film displays a larger specific capacitance of 738 F g^{-1}, lower resistance, and better stability as compared with the pure PANI film. Thus, good capacitive performance demonstrates its potential superiority for supercapacitors.

Keywords Polyaniline · Zinc ions · Electro-polymerization · Supercapacitor · Specific capacitance

Introduction

Electrochemical supercapacitors have been attracting much attention in many advanced power systems that require high power density, high specific energy, and excellent long-term cyclability, such as electric/hybrid vehicles, portable computers, cellular devices, and nanoelectronics [1–3]. In supercapacitors, active materials (i.e., carbon materials [4, 5], transition metal oxides [6, 7], and conducting polymers [8–10]) are the most important factor in adjusting the electrochemical performance. Among the active materials in most reports, conducting polymers offer advantages of lower cost in comparison with metal oxides and higher charge density, in contrast with carbon materials. Polyaniline (PANI) is an attractive candidate among the various conductive polymers based on its unique doping/de-doping behavior, intrinsic electrical conductivity, facile synthesis, and environmental stability [11–16], where its doping process is associated with inorganic acids (such as HCl, $HClO_4$, and H_2SO_4 [17, 18]) or organic acids (such as p-toluene sulfonic acid [19]). The doping/de-doping process involves redox reactions which are the basic of energy storage in doped PANI. Recently, the doping of PANI with transitional metal ions has been widely studied due to the unique electron exchange property of the combination. Dhibar et al. [20] synthesized PANI in pure and doped forms with various doping levels of $CuCl_2$ using in situ polymerization method, where PANI in doped form shows higher specific capacitance value of 626 F g^{-1} at 10 mV s^{-1} scan rate at 2 wt% doping level and has the higher thermal stability. Ghosh et al. [21] prepared H^+ and Fe^{3+} co-doped PANI/MWCNTs nanocomposites by in situ oxidative polymerization method, which obtained a higher specific capacitance of 575 F g^{-1} at a current density of 1 A g^{-1}. Li et al. [22] reported that PANI co-doped with Zn^{2+} and H^+ was synthesized in aqueous HCl solution containing $ZnCl_2$ by simple chemical oxidation polymerization, which showed a specific capacitance of 369 F g^{-1} at a current density of 0.1 A g^{-1}.

In previous works, we have demonstrated that PANI film doped with Ni^{2+} has a larger specific capacitance of

H. Xu (✉) · J. Zhang · Y. Chen · H. Lu · J. Zhuang
College of Petrochemical Technology, Lanzhou University of Technology, Lanzhou, China
e-mail: xuhui@lut.cn

658.3 F g^{-1} compared to pure PANI film [23]. In this research, the PANI doped with Zn^{2+} films was prepared via electropolymerization onto a stainless steel mesh. Impressively, the PANI/ Zn^{2+} films exhibited a quite good pseudo-capacitive performance with high capacitance.

Experiments

Materials

Aniline was vacuum-distilled at 120 °C and stored in a refrigerator before use. Other reagents and solvents were used without further purification.

Electrochemical deposition of PANI and PANI/Zn^{2+}

The materials of PANI and PANI/Zn^{2+} were prepared by cyclic voltammetric method in a classic one-compartment cell using a three-electrode configuration on CHI660B electrochemical work station. Saturated calomel electrode (SCE) was used as reference electrode, platinum sheet was used as counter electrode, and stainless steel mesh (325-mesh) was used as working electrode which had a deposited area of 1 cm^2 (1 cm×1 cm) with the opposite side coated with PTFE. The stainless steel mesh was ultrasonically washed with acetone, ethanol, and distilled water and was lastly air-dried. The cyclic voltammetry (CV) curves were recorded in a mixture of 0.5 mol L^{-1} H$_2$SO$_4$ and 0.2 mol L^{-1} aniline, doped with different concentrations of ZnSO$_4$·7H$_2$O (0.1, 0.2, 0.3, and 0.4 mol L^{-1}) for 71 cycles in the potential range of −0.2 to 0.9 V at a rate of 20 mV s^{-1}. After deposition, PANI/Zn^{2+} films were rinsed with 0.5 mol L^{-1} H$_2$SO$_4$ and dried in vacuum condition at 60 °C for 12 h. The pure PANI film was also prepared following the above procedure without the addition of ZnSO$_4$·7H$_2$O.

Structural characterizations

The structure of the sample was characterized by Fourier transform infrared (FT-IR; Nicolet, USA) with records between 4,000 and 400 cm^{-1}. The X-ray diffraction (XRD) patterns were characterized using an X-ray diffractometer (D/MAX-2400X) with Cu Kα radiation (λ=0.154056 nm) at a scanning rate of 5° min^{-1} in the 2θ range of 10°–90°. The morphology of PANI and PANI/Zn^{2+} was measured by scanning electron microscopy (SEM; JEOL JSM-6701 F). Elemental analysis was performed by energy-dispersive X-ray spectroscopy (EDS; JEOL JSM-5600LV). The X-ray photoelectron spectroscopy (XPS) data was obtained by a V.G. ESCA Laboratory 210 photoelectron spectrometer with Mg Kα source, and the spectra were acquired with a 30-eV pass energy.

Electrochemical tests

All electrochemical tests were carried out on the CHI660B electrochemical work station in a three-electrode glass cell with PANI and PANI/Zn^{2+} films as working electrode, platinum plate as counter electrode, and standard calomel as reference electrode. The electrolyte was a 0.5-mol L^{-1} H$_2$SO$_4$ solution. Cyclic voltammetry and galvanostatic charge–discharge tests were performed in the voltage window ranging from 0 to 0.7 V vs. SCE was at various scan rates from 3 to 20 mV s^{-1}. Electrochemical impedance spectroscopy (EIS) measurements were recorded in the range of 10^5–10^{-2} Hz with an excitation signal of 4 mV.

Results and discussion

Fourier transform infrared spectroscopy

The structure of PANI and PANI/0.4 M Zn^{2+} films prepared in the solution with 0.4 mol L^{-1} Zn^{2+} was measured by Fourier transform infrared (FT-IR) spectroscopy. Figure 1(a) shows the characteristic peaks at 1,558, 1,470, 1,298, 1,234, 1,118, and 804 cm^{-1}, indicating the backbone of pure PANI [24]. However, as seen in Fig. 1(b), some peaks of PANI/0.4 M Zn^{2+} have shifted slightly due to the interaction between Zn^{2+} and PANI nanoparticles. The peaks at 1,558 and 1,470 cm^{-1} are shifted to 1,559 and 1,472 cm^{-1}, respectively, indicating the conversion between the quinoid rings and the benzenoid ring by a proton-induced spin unpairing mechanism, which is deemed to be used on PANI backbone for increasing the degree of charge delocalization [25]. Also, the peaks at 1, 298, 1,234, and 1,118 cm^{-1} shifted to 1,300, 1,230, and 1, 123 cm^{-1}, respectively, which indicates that the doping of PANI with Zn^{2+} is a pseudo-protonation of the imine nitrogen. The peaks that changed from 804 to 801 cm^{-1} show a red shift in PANI/0.4 M Zn^{2+}, which indicates the interaction between PANI chains and zinc ions [26].

XRD studies

Figure 2 shows the X-ray diffraction spectra of PANI and PANI/ 0.4 M Zn^{2+} films. In pure PANI (Fig. 2(a)), one broad peak can be observed at 2θ=21.4°, which is attributed to the amorphous PANI. In Fig. 2(b), two peaks can be observed at 2θ=20.5°, corresponding to the alternating distance between layers of polymer chains, and at 2θ=25.4°, attributed to the periodicity that is perpendicular to the chain of PANI/0.4 M Zn^{2+} [27], which confirms the lower crystallinity and conductive emeraldine–salt structure of PANI/0.4 M Zn^{2+}.
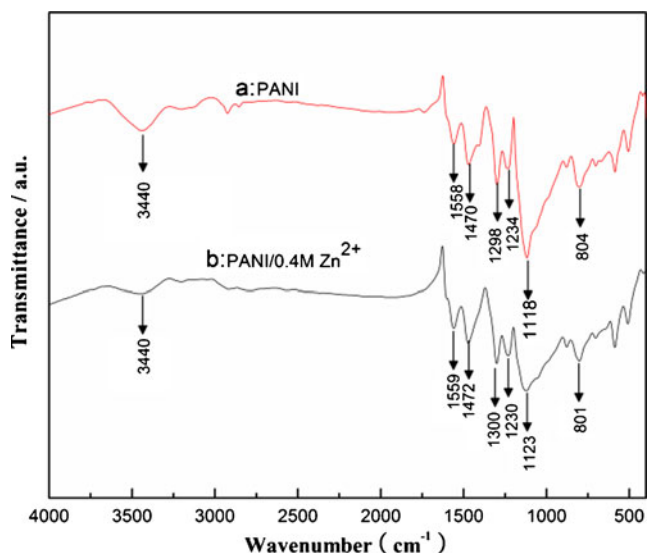
Fig. 1 FT-IR spectra of (*a*) PANI film and (*b*) PANI/0.4 M Zn^{2+} film prepared in the solution with 0.4 mol L^{-1} Zn^{2+}

SEM characterization

The morphologies of PANI and PANI/0.4 M Zn^{2+} films were characterized by SEM, as shown in Fig. 3. Figure 3a, b shows the pure PANI having a nanorod structure with a size of 1 μm. Similarly, PANI/0.4 M Zn^{2+} shows a nanorod structure (Fig. 3c, d) and a surface roughness with aggregated of nanoparticles, which can effectively contribute to the redox reaction of the electrolyte in the PANI/0.4 M Zn^{2+} electrode. The reason could be due to transitional metal ions such as Zn^{2+} having multiple doping positions, as proven by FT-IR, which may bind to several nitrogen sites in PANI chains or form inter-chain linkages among several adjacent PANI chains by coordination [28].
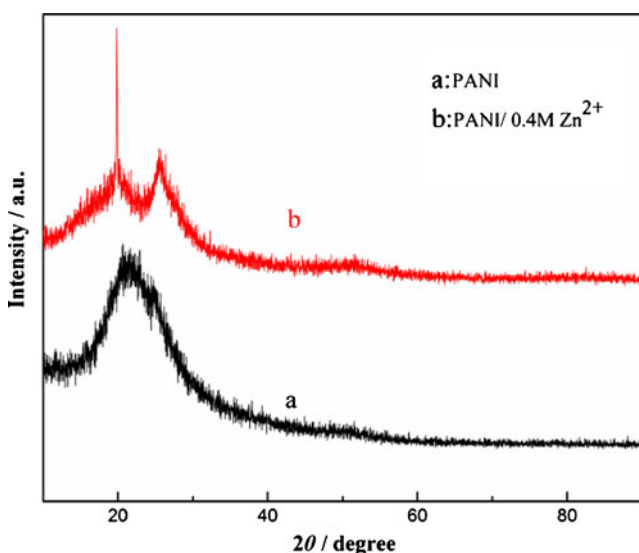

Fig. 2 XRD patterns of (*a*) PANI film and (*b*) PANI/0.4 M Zn^{2+} film prepared in the solution with 0.4 mol L^{-1} Zn^{2+}

EDS and XPS analyses

Figure 4 shows the EDS of the PANI/0.4 M Zn^{2+} film. The deposited PANI/0.4 M Zn^{2+} film is composed of C, N, O, S, and Zn elements, with Zn=12.43 wt%. The chemical valence of Zn in the PANI/0.4 M Zn^{2+} film was investigated by XPS. From Fig. 5, two main peaks appear at 1,023.4 and 1046.4 eV, which can be assigned to Zn $2p_{3/2}$ and Zn $2p_{1/2}$, respectively; it confirms the presence of Zn^{2+} ions [29, 30].

## Electrochemical characterizations

Cyclic voltammetry test

Considering that the electrode material exhibited the best electrochemical behavior, a potential window ranging from 0 to 0.7 V was chosen for the cyclic voltammetry measurements. Figure 6 shows the CV curves of PANI and PANI/Zn^{2+} film electrodes at a scan rate of 5 mV s^{-1}. The CV curves of PANI/Zn^{2+} films are similar to that of the PANI film, but the existence of Zn^{2+} increases a shift in the oxidation and reduction peaks. The areas of CV curves of the PANI/Zn^{2+} films are larger than that of PANI films, indicating the larger specific capacitance of PANI/Zn^{2+} films, which can be attributed to the effect of zinc ions in the formation of charge transfer complex with the PANI chains. The insertion of Zn^{2+} in the conductive polymer usually takes place on the bulk volume of the material rather than on the surface, which can be explained as the π electron donation phenomenon from PANI to the Zn^{2+}.

To better understand the redox mechanism occurring in the PANI/0.4 M Zn^{2+} film electrode, the CV tests were performed over a wide range of scan rates. The CV plots of the PANI/0.4 M Zn^{2+} film at various scan rates of 3, 5, 10, and 20 mV s^{-1} are shown in Fig. 7, where three pairs of redox peaks can be observed (P_1/P_1', P_2/P_2', and P_3/P_3'), which correspond to the leucoemeraldine–emeraldine transformation (P_1/P_1', 0.19/0.01 V), the degradation of PANI salts (P_2/P_2', 0.52/0.36 V) and the emeraldine–pernigraniline transformation (P_3/P_3', 0.7/0.6 V), respectively. The scan rate has an effect on the diffusion of electrolyte ions on the exterior and interior materials of the electrode during potential cycling. The electrolyte ions have difficulty diffusing into the interior material of the stainless steel mesh electrode with the increasing scan rate. The increase in scan rate leads to the change of the shape of CV curves, which deviates from rectangular form and increases the current density. It can be attributed to the IR drop.

Galvanostatic charge–discharge experiments

The galvanostatic charge–discharge studies are the most direct approach to evaluate the applicability of supercapacitors. The specific capacitance has been believed to approach full

Fig. 3 SEM images of PANI
(**a**, **b**) and PANI/0.4 M Zn^{2+}
(**c**, **d**) prepared in the solution
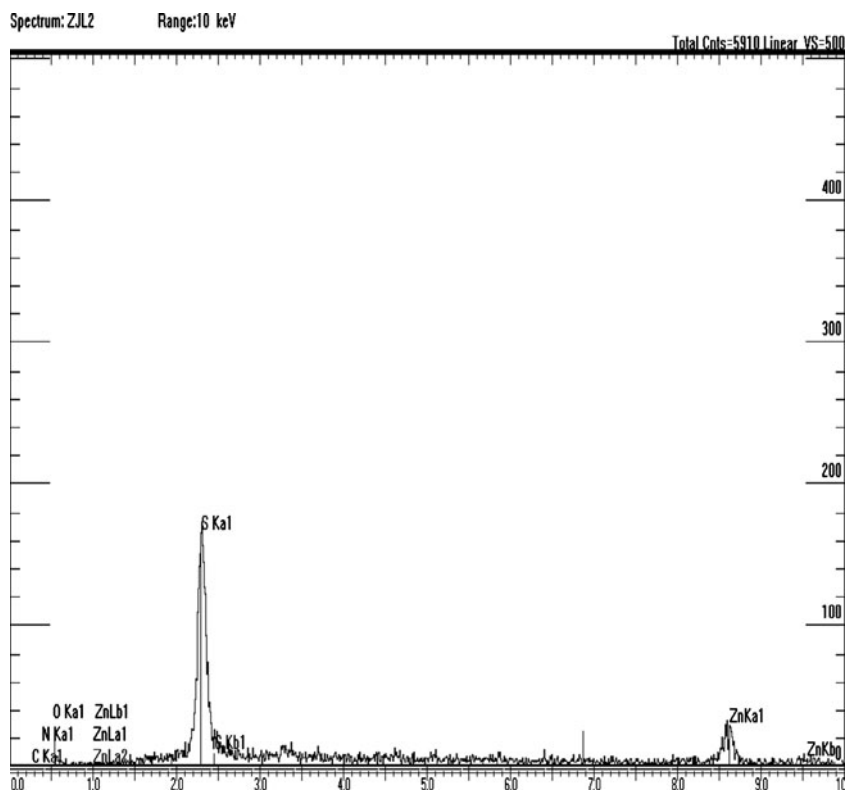with 0.4 mol L^{-1} Zn^{2+}
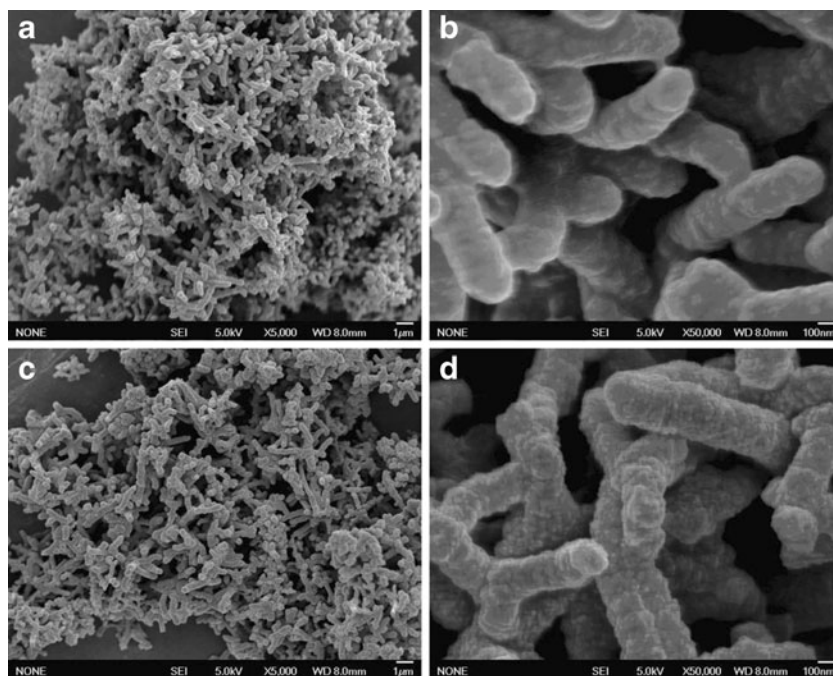
utilization of the electrode material at low current density [31, 32], so the galvanostatic charge–discharge experiments were first measured at a constant current density of 5 mA cm^{-2}. Figure 8 shows that the charge and discharge profiles of PANI and PANI/Zn^{2+} electrodes exhibit a slight curve, which is a pseudo-capacitive characteristic. The discharge-specific

capacitance is derived from the discharge curve using the following formula [23]:

$$C_m = \frac{c}{m} = \frac{I\Delta t}{m\Delta V},$$

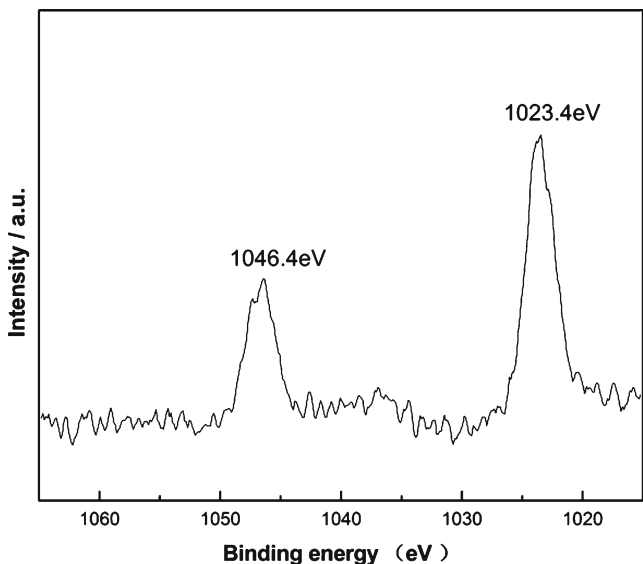Fig. 4 EDS of the PANI/0.4 M Zn^{2+} film prepared in the solution with 0.4 mol L^{-1} Zn^{2+}

Fig. 5 XPS spectra of Zn 2p in the PANI/0.4 M Zn²⁺ film prepared in the solution with 0.4 mol L⁻¹ Zn²⁺

Fig. 7 CV curves of PANI/0.4 M Zn²⁺ film prepared in the solution with 0.4 mol L⁻¹ Zn²⁺ at different scan rates

where C_m is specific capacitance (F g⁻¹), I is the charge/discharge current (A), Δt is the discharge time after IR drop (s), ΔV is the potential drop in the discharge progress (V), and m denotes the mass of active material (6 mg). The calculated specific capacitance values are 542, 608, 629, 719, and 738 F g⁻¹ for PANI, PANI/0.1 M Zn²⁺, PANI/0.2 M Zn²⁺, PANI/0.3 M Zn²⁺, and PANI/0.4 M Zn²⁺, respectively. As shown in Fig. 9, with the increasing concentration of Zn²⁺, the specific capacitance increases from 542 to 738 F g⁻¹, which may be due to the fact that the presence of Zn²⁺ provides a path of least resistance to electrons. Zn²⁺ can own a coordination number of less than four which means that one of the Zn²⁺ ions may bind to more than one imine nitrogen sites in PANI chains or form inter-chain linkages among several
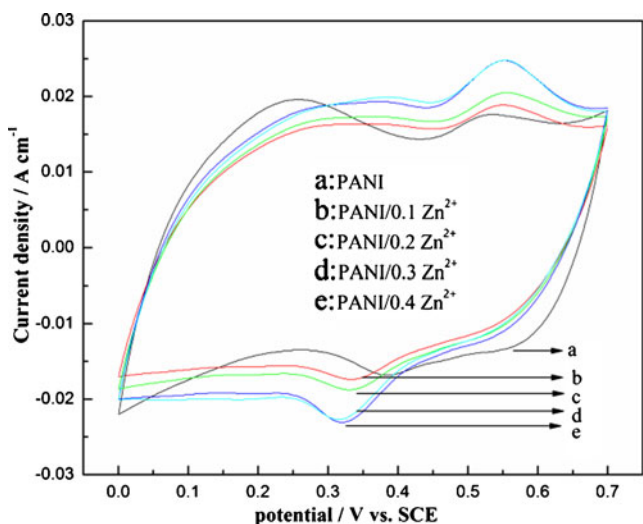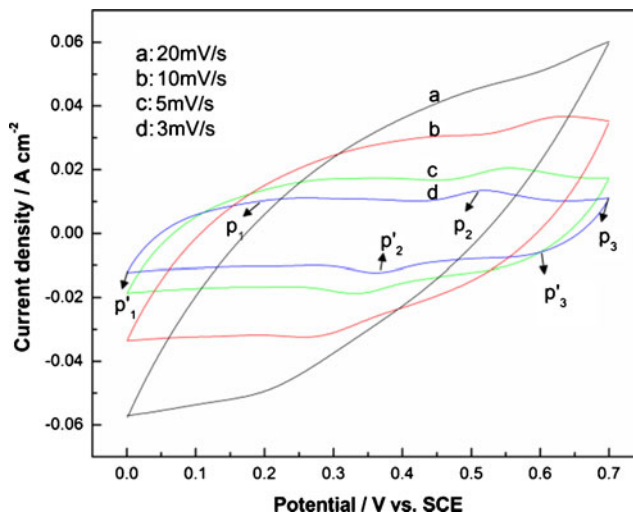
adjacent PANI chains by coordination, which leads to a more effective conjugated network or matrix [22].

The charge–discharge measurement of the PANI/0.4 M Zn²⁺ (Fig. 10) was also performed at various current densities of 3, 5, 10, and 20 mA cm⁻² in 0.5-mol L⁻¹ H₂SO₄ electrolyte; on the basis of the above equation, the calculated specific capacitance values are 718, 738, 702, and 624 F g⁻¹, respectively. The anodic charge curves show mirror symmetry to their cathodic discharge counterparts at each current density, indicating excellent electrochemical performance. With the increasing of charge–discharge current densities, a potential drop rapidly increased due to electrode polarization and internal resistance. However, the IR drop is not obvious at a relatively low current density. With the decrease of charge–discharge current densities, the anodic charge curves deviate from the straight lines, which also may be caused by electrode polarization and internal resistance [33].
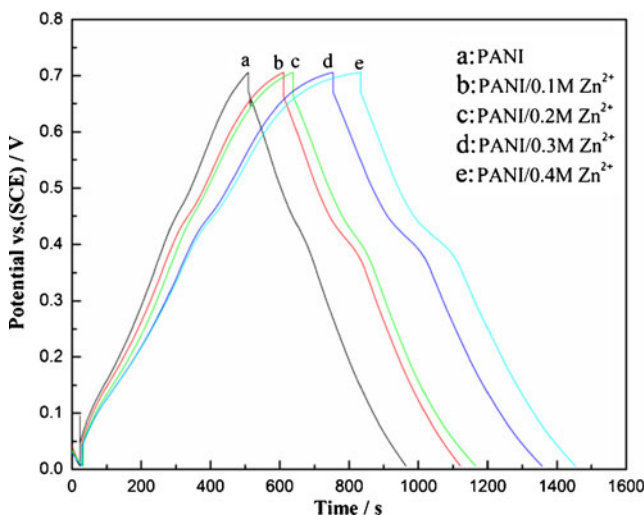

Fig. 6 CV curves of (*a*) PANI and (*b*, *c*, *d*, *e*) PANI/Zn²⁺ films at a scan rate of 5 mV s⁻¹ in 0.5 mol L⁻¹ H₂SO₄

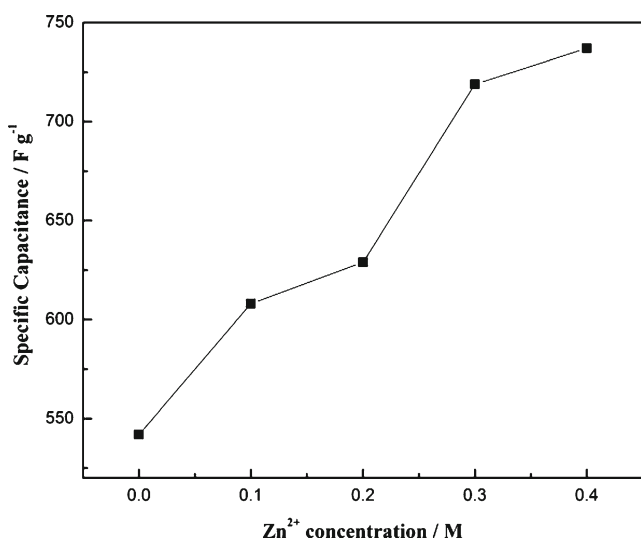**Fig. 8** Charge–discharge curves of (*a*) PANI and (*b*, *c*, *d*, *e*) PANI/Zn²⁺ films at a current density of 5 mA cm⁻²

Fig. 9 Variation of specific capacitance with respect to Zn^{2+} concentration at a current density of 5 mA cm^{-2}

Fig. 11 Variation of discharge-specific capacitance of (*a*) PANI and (*b*) PANI/0.4 M Zn^{2+} film prepared in the solution with 0.4 mol L^{-1} Zn^{2+} as a function of cycle number at 5 mA cm^{-2}

The long-term cycle stability of the composites was calculated by repeating the charge–discharge cycling tests in 0.5-mol L^{-1} H$_2$SO$_4$ electrolyte at a scan rate of 5 mV s^{-1} for 500 cycles. In Fig. 11, the variation of specific capacitance with cycle numbers at 5 mA cm^{-2} indicates the final specific capacitance retention of 45 and 63 % for PANI and PANI/0.4 M Zn^{2+} films. Due to the degradation of incompletely formed polymers or some un-doped PANI, the materials initially exhibit a quick decrease of specific capacitance. Compared with specific capacitance retentions, Zn^{2+} has a positive effect on the cyclability of PANI due to the network or matrix of PANI chains with Zn^{2+} doping, which takes better synergy of volume changes of the redox process into consideration. Meanwhile, the nanometer dimension of PANI/Zn^{2+} has a reducing effect on the diffusion resistance of the electrolyte ions within the electrode [23, 34].
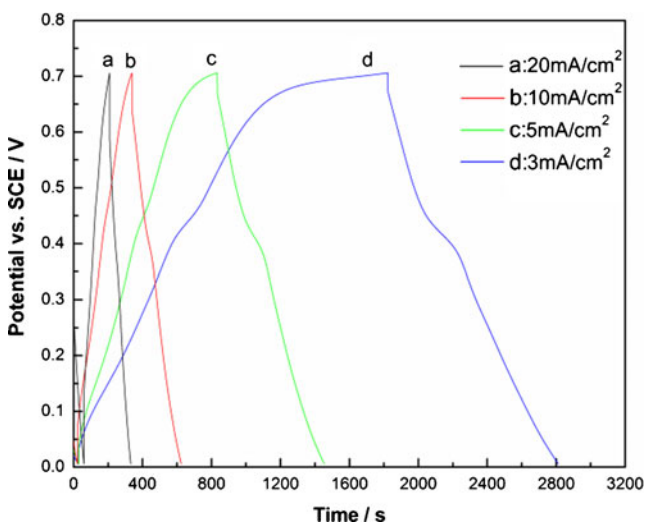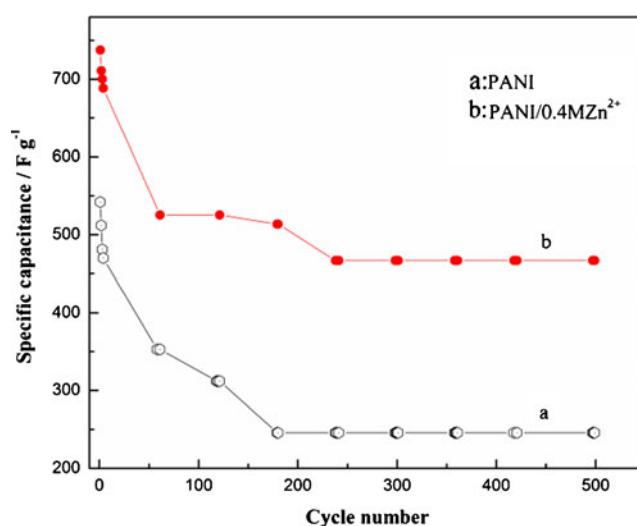
Electrochemical impedance spectroscopy

Figure 12 shows the Nyquist plots of impedance for PANI and PANI/Zn^{2+} films. The Nyquist plots of impedance give information about the electrochemical impedance behavior of the PANI and PANI/Zn^{2+} films. The real component (Z') stands for the ohmic properties, and the imaginary component (Z'') represents the capacitive properties [35]. The EIS measurements were carried out at a constant potential of 0.4 V. The solution resistance of the composites can be obtained from the intercepts in the highest frequency of the curves at the real axis. The diameter of the semicircle provides a value of the charge transfer resistance (Rct) at the electrode/electrolyte interface, which depends on ion diffusion in the electrolyte to the electrode interface. The tilted straight line in the low-
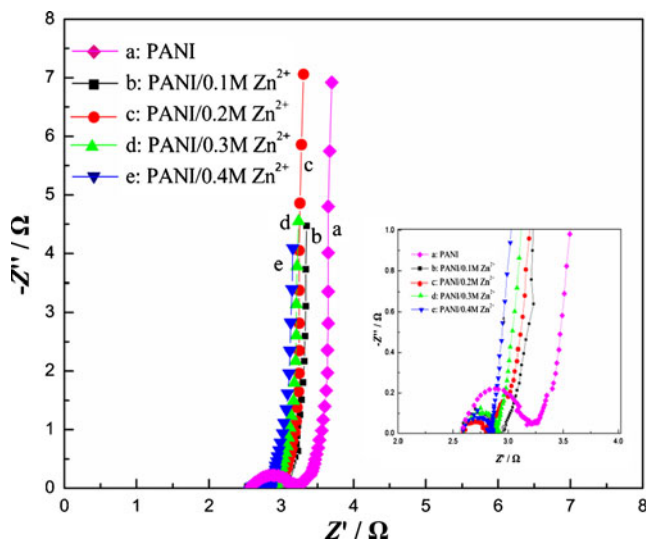

Fig. 10 Charge–discharge curves of (*a*, *b*, *c*, *d*) PANI/0.4 M Zn^{2+} at various current densities

Fig. 12 EIS of (*a*) PANI and (*b*, *c*, *d*, *e*) PANI/Zn^{2+} films at an open-circuit potential of 0.4 V

frequency region represents a limiting diffusion process in the H_2SO_4 electrolyte, which exhibits the characteristic of an ideal capacitive behavior. As can be seen in Fig. 12, the solution resistance of the composites is obviously found at $2.6\,\Omega$. The $\pi-\pi$ interaction between Zn^{2+} and PANI may be the possible reason behind the low solution resistance value which allows efficient electrolyte accessibility to the electrode surface. The charge transfer resistances estimated from the diameter of the semicircles are 0.6, 0.3, 0.2, 0.3, and $0.3\,\Omega$ with the increasing concentration of zinc ions, respectively. Moreover, the irregular semicircle that can be seen in Fig. 12 (inset) is due to the inhomogeneity on the surface of the electrode and the complexity of interface structure. In general, the semicircle diameter of PANI/Zn^{2+} is smaller than that of PANI, indicating that the doping of Zn^{2+} ions has a positive effect on shortening the ion diffusion path which contributes to the effective access of electrolyte ions to the electrode surface. The almost vertical line suggests the ideally capacitive behavior of the electrodes.

Conclusions

In summary, PANI doped with Zn^{2+} was synthesized by electro-polymerization onto the stainless steel mesh. Different from pure PANI, the PANI/Zn^{2+} films show a larger specific capacitance of 738 F g^{-1} at a current density of 5 mA cm^{-2} and lower resistance. The properties are mainly attributed to the $\pi-\pi$ interaction between Zn^{2+} and PANI. The zinc ions play a positive role in the PANI, which can be considered as a potential and effective way to improve the performance of supercapacitors.

References

1. Sarangapani S, Tilak BV, Chen CP (1996) J Electrochem Soc 143:3791–3799
2. Winter M, Brodd RJ (2004) Chem Rev 104:4245–4269
3. Zheng L, Wang X, An H, Wang X, Yi L, Bai L (2011) J Solid State Electrochem 15:675–681
4. Pandolfo AG, Hollenkamp AF (2006) J Power Sources 157:11–27
5. Cabezas AL, Zhang ZB, Zheng LR, Zhang SL (2010) Synth Met 160:664–668
6. Toupin M, Brousse T, Bélanger D (2004) Chem Mater 16:3184–3190
7. Huo Y, Zhang H, Jiang J, Yang Y (2012) J Mater Sci 47:7026–7034
8. Ryu KS, Kim KM, Park NG, Park YJ, Chang SH (2002) J Power Sources 103:305–309
9. Xing S, Zhao C, Jing S, Wang Z (2006) Polymer 47:2305–2313
10. Yu G, Hu L, Vosgueritchian M, Wang H, Xie X, McDonough JR, Cui X, Cui Y, Bao Z (2011) Nano Lett 11:2905–2911
11. An H, Wang Y, Wang X, Li N, Zheng L (2010) J Solid State Electrochem 14:651–657
12. Sariciftci NS, Bartonek M, Kuzmany H, Neugebauer H, Neckel A (1989) Synth Met 29:193–202
13. Mi HY, Zhang XG, Yang SD, Ye XG, Luo JM (2008) Mater Chem Phys 112:127–131
14. Mi HY, Zhang XG, Ye XG, Yang SD (2008) J Power Sources 176:403–409
15. Girija TC, Sangaranarayanan MV (2006) J Power Sources 156:705–711
16. Gupta V, Miura N (2005) Electrochem Solid-State Lett 8:A630–A632
17. Wang C, Sun L, Zhou Y, Wan P, Zhang X, Qiu J (2013) Carbon 59:537–546
18. Pahovnik D, Žagar E, Kogej K, Vohlidal J, Žigon M (2013) Eur Polym J 49:1381–1390
19. Xu G, Wang W, Qu X, Yin Y, Chu L, He B, Wu H, Fang J, Bao Y, Liang L (2009) Eur Polym J 45:2701–2707
20. Dhibar S, Sahoo S, Das CK, Singh R (2013) J Mater Sci 24:576–585
21. Ghosh D, Giri S, Mandal A, Das CK (2013) Appl Surf Sci 276:120–128
22. Li J, Cui M, Lai Y, Zhang Z, Lu H, Fang J, Liu Y (2010) Synth Met 160:1228–1233
23. Xu H, Li J, Peng Z, Zhuang J, Zhang J (2013) Electrochim Acta 90:393–399
24. Tao S, Hong B, Kerong Z (2007) Spectrochim Acta Part A 66:1364–1368
25. Chiang JC, MacDiarmid AG (1986) Synth Met 13:193–205
26. Chen SA, Lin LC (1995) Macromolecules 28:1239–1245
27. Moon YB, Cao Y, Smith P, Heeger AJ (1989) Polymer Communications 30:196–199
28. Yang C, Chen C (2005) Synth Met 153:133–136
29. Milenova K, Stambolova I, Blaskov V, Eliyas A, Vassilev S, Shipochka M (2013) Journal of Chemical Technology and Metallurgy 48:259–264
30. Liu Y, Yang SH, Zhang YL, Bao DH (2009) J Magn Magn Mater 321:3406–3410
31. Li GR, Feng ZP, Zhong JH, Wang ZL, Tong YX (2010) Macromolecules 43:2178–2183
32. Patil DS, Shaikh JS, Pawar SA, Devan RS, Ma YR, Moholkar AV, Kim JH, Kalubarme RS, Park CJ, Patil PS (2012) Phys Chem Chem Phys 14:11886–11895
33. Wang YG, Xia YY (2006) J Electrochem Soc 153:450–454
34. Zhang H, Cao G, Wang W, Yuan K, Xu B, Zhang W, Cheng J, Yang Y (2009) Electrochim Acta 54:1153–1159
35. Chen W, Rakhi RB, Hu L, Xie X, Cui Y, Alshareef HN (2011) Nano Lett 11:5165–5172